more attention as a possible energy source that could have a significant impact in areas such as the U.S. Gulf Coast, where brine and fresh water or seawater exist in abundance.

MARK OLSSON
Institute of Marine Resources, Scripps Institution of Oceanography, University of California, San Diego, La Jolla 92093, and *Foundation for Ocean Research, San Diego 92121*
GERALD L. WICK
Institute for Transcultural Studies, Los Angeles, California 90006
JOHN D. ISAACS
Institute of Marine Resources, Scripps Institution of Oceanography, and *Foundation for Ocean Research*

References and Notes

1. G. L. Wick and J. D. Isaacs, *Utilization of Energy from Salinity Gradients* (IMR 76-9, Institute of Marine Resources, University of California, La Jolla, 1976).
2. S. Loeb, *Science* **189**, 654 (1975).
3. G. L. Wick and J. D. Isaacs, *ibid.* **199**, 1436 (1978); *ibid.* **203**, 376 (1979).
4. G. L. Wick and W. R. Schmitt, *Mar. Technol. Soc. J.* **11**, 16 (1977).
5. S. Loeb, *J. Membr. Sci.* **1**, 49 (1976); Inter-Technology/Solar Corporation, *Solar Electricity: Osmo-hydro Power from Aqueous Saline Solutions, Assessment of Its Potential* (Report 289378, Department of Energy, Washington, D.C., 1978).
6. J. Weinstein and F. Leitz, *Science* **191**, 557 (1976).
7. B. W. Tleimat, paper presented at the American Society of Mechanical Engineers Winter Annual Meeting, Los Angeles, 16–20 November 1969.
8. A. Laird, personal communication.
9. G. Claude, *Mech. Eng.* **52**, 1039 (1930).
10. C. E. Brown and L. Wechsler, in *Proceedings of the Seventh Annual Offshore Technology Conference* (1975), vol. 2, p. 111.
11. *Proceedings of the Fifth Ocean Thermal Energy Conversion Conference* (Conf. 780236, Department of Energy, Washington, D.C., 1978).
12. G. L. Wick, *Energy Int. J.* **3**, 95 (1978).
13. Carnot efficiency applies to the latent heat transferred back to the evaporation chamber.
14. This estimate of power was conservative, since the useful energy was not extracted by a turbine in these experiments. This energy thus appeared as heat on the saltwater side and tended to oppose the vapor transfer.
15. We thank the trustees of the Foundation for Ocean Research for their support, S. Sinell for assisting in the experiments, and R. Ando for valuable discussions. This research was partially supported by grant 04-6-158-4410 (project R/E-6) from the Office of Sea Grant, National Oceanic and Atmospheric Administration.

27 March 1979; revised 4 June 1979

Zonal Temperature-Anomaly Maps of Indian Ocean Surface Waters: Modern and Ice-Age Patterns

Abstract. *Maps of sea surface temperature anomalies in the Indian Ocean in modern and ice-age times reveal striking changes in its surface circulation. During the last glacial maximum (18,000 years before the present), the Indian Ocean had colder average zonal surface temperatures, a cooler and less extensive Agulhas Current, a distinct eastern boundary current, and decreased upwelling and a weaker southwest monsoon in its northwestern region.*

Maps of zonal anomalies in the temperature of the sea's surface can be a valuable tool in interpreting major circulation features in the modern ocean (*1–3*). We have used such maps to interpret the surface circulation of the Indian Ocean during the last glacial maximum [18,000 years before present (B.P.)]. Paleoceanographic studies have been made in which various faunal or floral indicators were used to chart the spatial variation of water masses in the past. In the CLIMAP program, which was formed in 1971 to study the history of global climate, scientists have estimated sea surface temperatures (SST's) in the past from biotic components of deep-sea sediments and mapped them on a time horizon of 18,000 years B.P. (*4, 5*). Maps of modern and ice-age SST's reflect current systems and water masses; maps of the temperature differences between them can be useful in interpreting the oceanic response to climatic change (*4*). In this report we compare zonal SST anomaly maps of the Indian Ocean in modern and ice-age times to obtain additional information on how ice-age surface water circulation may have been different.

Zonal SST anomalies (ΔSST_z) are calculated as follows:

$$\Delta SST_z = (SST - \overline{SST}_z)$$

where SST is the temperature at points along a latitudinal band and $\overline{SST}_z$ is the average temperature of the latitudinal band. Seasonal ΔSST_z maps of the Indian Ocean today and 18,000 years B.P. were constructed by using a grid spacing of 2° of longitude and averaging along a zonal width of 2° of latitude. Because flow is primarily zonal south of the Subtropical Convergence, only anomalies north of the convergence (that is, north of 50°S, between 20° and 120°E) are reported.

The data we used to construct ΔSST_z represent sea surface conditions for the Indian Ocean in both times. Data for present-day February and August SST's are shown in Fig. 1, A and B (*6*). Isotherms for the last glacial maximum (Fig. 1, C and D) are based on 42 SST estimates from planktonic foraminiferal transfer function FI-2 (*7*), faunal province boundaries, and analogies to modern SST gradients. The standard error of individual estimates for FI-2 is ± 1.1°C for February and ± 1.3°C for August. However, adjacent cores in low-gradient areas normally differ by $<\pm$ 0.5°C. Accordingly, although we feel that the distribution of data points (Fig. 1) and the smoothness of gradients precludes major errors, we have not placed great emphasis on interpreting ΔSST_z of < 1°C. South of the Subtropical Convergence, additional data based on radiolaria (*8*) support the gradients determined from the estimates based on foraminifera. The February and August ΔSST_z maps for modern and ice-age times are shown in Fig. 2.

Maps of ΔSST_z reveal temperature contrast along a zonal band and identify areas that are colder or warmer than the latitudinal average. If there were no large ocean currents and continental boundaries, ocean surface temperatures would reflect the pattern of solar radiation and show meridional temperature gradients. Isotherms would be zonal and all temperatures along a latitudinal zone would be equal; ΔSST_z would be zero. In the real ocean, however, current systems and continental boundaries preclude so simple a zonal pattern. Anomalies are created by advection of warm or cold waters into a latitudinal zone. In general, horizontal advection transports warm waters poleward, producing positive anomalies (for example, the Gulf Stream) along western boundaries, and transports cold waters equatorward, producing negative anomalies (for example, the Peru Current) along eastern boundaries. In addition, vertical advection brings cold water to the surface, creating negative anomalies along some continental margins. Thus, a map of ΔSST_z should reflect these circulation features.

The maps of ΔSST_z in the Indian Ocean for February and August in modern times (Fig. 2, A and B) reveal the major circulation features north of the Subtropical Convergence. Examination of Fig. 2A reveals that in February (i) a large positive ΔSST_z southeast of Africa coincides with the southerly flowing Agulhas Current; (ii) in the eastern section of the subtropical gyre, equatorward flow (indicated by negative ΔSST_z's) is centered at approximately 105°E; (iii) across the central Indian Ocean, negative anomalies trend from southeast to northwest and generally coincide with the South Equatorial Current; and (iv) north of the equator, the northwestern Indian Ocean

0036-8075/79/1026-0454$00.50/0

has negative ΔSST_z's (possibly caused by the winter Somali Current) and the northeast has positive ΔSST_z's; however, no anomalies are more than 1°C.

The map for August (Fig. 2B) shows that:

1) Large positive anomalies (> 3°C) occur in the area of the Agulhas Current. These anomalies are larger than the ΔSST_z's in February and reflect greater equatorward flow of cold water in the eastern sector during winter in the Southern Hemisphere.

2) In the eastern section of the subtropical gyre, negative anomalies associated with equatorward flow are centered at 90°E, and positive ΔSST_z's occur along Australia. These ΔSST_z patterns are consistent with charts of surface currents, which show poleward currents along the western coast of Australia and equatorward flow farther offshore (*9*).

3) A continuous band of negative ΔSST_z's extends northwestward across the Indian Ocean.

4) Large negative ΔSST_z's (− 3°C) occur near the Somalia and Arabian peninsulas and reflect strong upwelling associated with the southwest monsoon. These large negative anomalies are the most striking difference between the maps of the Indian Ocean in August and in February.

These maps show patterns that are, in part, functions of the major circulation systems within the Indian Ocean and they outline their relative seasonal intensity. Because we are primarily interested in the differences between modern and ice-age circulation, we have not calculated the difference between an idealized zonal model and the modern ocean. Rather, we used the maps of present-day ΔSST_z's as a baseline against which to measure changes in ΔSST_z since 18,000 years B.P.

Initial examination of the ice-age ΔSST_z maps reveals gross similarities to the modern ΔSST_z patterns. However, detailed comparison of zonal averages and ΔSST_z (Fig. 2) reveals four striking differences between ice-age and modern patterns which are indicative of major changes in the position and intensity of surface circulation.

First, SST was colder on the average at 18,000 years B.P. The average ice-age zonal SST for the entire Indian Ocean was 1.4°C cooler during February and 1.5°C cooler during August. However, between 30° and 50°S, the difference between ice-age and modern mean zonal SST's ranges from − 2° to − 5°C, reflecting a slight equatorward shift of the Subtropical Convergence (*10*) and a general cooling of the middle latitudes.

Second, at 18,000 years B.P. the positive ΔSST_z's associated with the Agulhas Current were less extensive and shifted somewhat farther south than today (Fig. 2, C and D). These patterns of reduced anomalies probably reflect less poleward transport of warm equatorial waters from the Agulhas Current. The anomalies also indicate a cooler midlatitude zone and Agulhas Current at 18,000 years B.P. (*7*). If the SST and transport values of the Agulhas Current during the ice age were similar to its modern values, more positive ΔSST_z's would be expected because the eastern Indian Ocean was colder and thus had greater zonal temperature contrast. The colder temperatures (indicated by the sharp eastward shift of the 0° anomaly) are probably responsible for the small positive anomalies near 30°S in the Agulhas Current region (Fig. 2, C and D). The Agulhas Current probably persisted as a west-

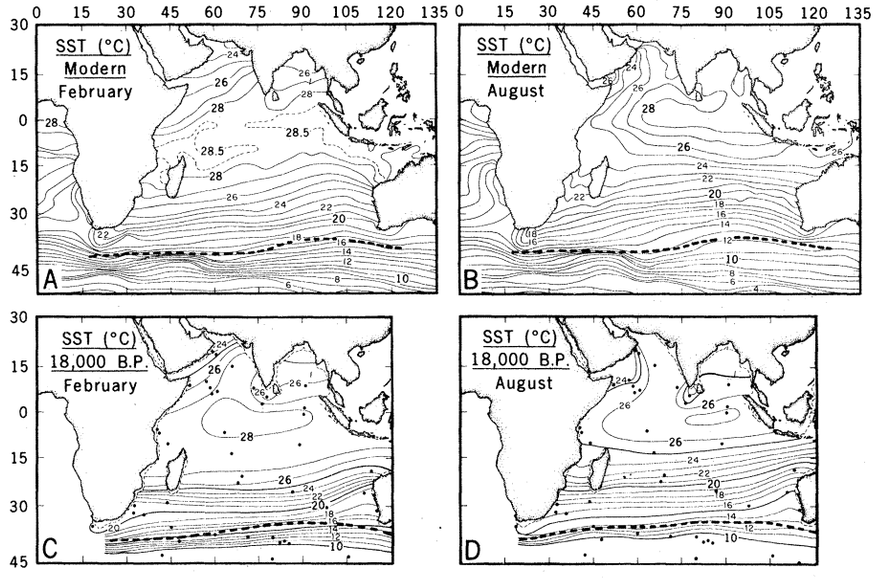

Fig. 1. Maps of SST for February (A) and August (B) in modern times (*6*) and estimates of SST for February (C) and August (D) at 18,000 years B.P. (*7*). Closed circles show location of deep-sea samples and SST estimates for 18,000 years B.P. (based on FI-2). The dashed line gives the position of the Subtropical Convergence (*7*, *10*).

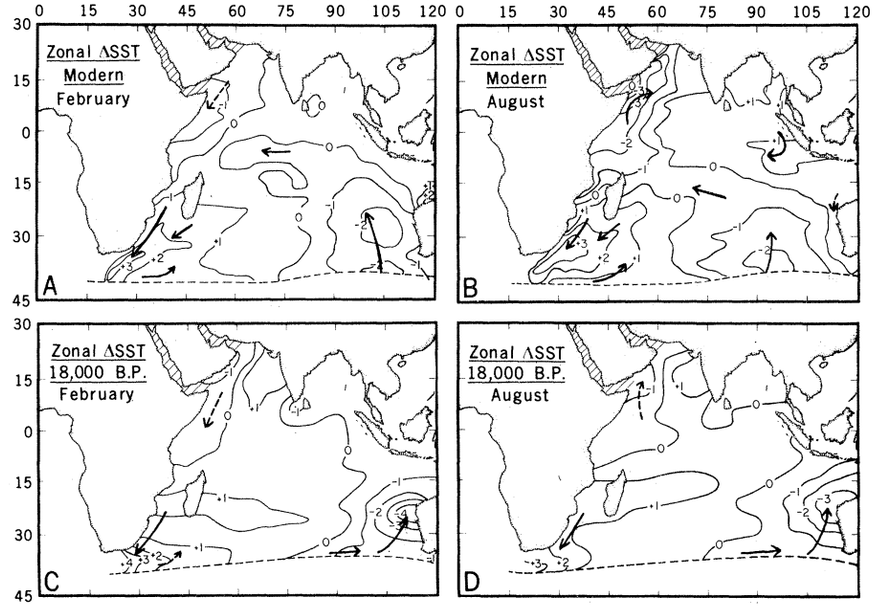

Fig. 2. Maps of zonal anomalies of SST (in degrees Celsius) for February (A) and August (B) in modern times and of estimates of SST for February (C) and August (D) at 18,000 years B.P. The dashed line gives the location of the Subtropical Convergence (*10*). Solid arrows show major currents; dotted arrows indicate weak or poorly defined currents.

ern boundary current during the last glacial maximum, but its SST's were lower than those today and its transport may have been less. The anomaly patterns also imply that more of the Agulhas is entrained in the West Wind Drift during February than in August.

Third, maps of ΔSST_z at 18,000 years B.P. (Fig. 2, C and D) show that equatorward flow (negative ΔSST_z's) around the subtropical gyre occurred as a distinct eastern boundary current along Australia, whereas today the return flow is concentrated offshore between 90° and 105°E. This observation is consistent with the suggestion of Prell *et al.* (*10*) that since the Subtropical Convergence was located at about 35°S at 18,000 years B.P., easterly flowing water (associated with the West Wind Drift) would be deflected equatorward along the coast of Australia. This northward advection would produce the negative ΔSST_z's along the coast. Webster and Streten (*11*) have come to a similar conclusion based on the more equatorward position of sea ice and the westerlies during the last glacial maximum.

Finally, large negative ΔSST_z's did not occur in the northwestern Indian Ocean during August at 18,000 years B.P. (Fig. 2D). The lack of these negative anomalies indicates less upwelling then than today. Decreased upwelling, in turn, implies that the southwest monsoon was weaker then. During this interval, the Somali Current was also weak and may even have flowed southward. These results are supported by faunal indicators of upwelling (*7, 12*) and by several general circulation model simulations of the ice-age atmosphere (*13, 14*). Furthermore, because monsoon intensity is influenced more by increased continental albedo than by reduced SST (*14*), this anomaly pattern confirms the simulation of the weak ice-age monsoon by Manabe and Hahn (*14*).

Maps of zonal anomalies of SST can be used to identify circulation patterns in modern oceans and their ancient counterparts. Although the mapping technique is highly informative, it requires quantitative estimates of SST on a synchronous basis and accurate plotting of isotherms. Properly drawn, the ΔSST_z map reflects the thermal contrast across an ocean basin and thus the dominant circulation patterns.

WARREN L. PRELL
CLIMAP, *Department of Geological Sciences, Brown University, Providence, Rhode Island 02912*
WILLIAM H. HUTSON
CLIMAP, *School of Oceanography, Oregon State University, Corvallis 97331*

References and Notes

1. G. Neumann and W. J. Pierson, Jr., *Principles of Physical Oceanography* (Prentice-Hall, Englewood Cliffs, N.J., 1966).
2. R. G. Barry and R. J. Chorley, *Atmosphere, Weather, and Climate* (Holt, Rinehart & Winston, New York, 1970).
3. A. Defant, *Physical Oceanography* (Pergamon, New York, 1961), vol. 1, p. 645.
4. CLIMAP Project Members, *Science* **191**, 1131 (1976).
5. R. M. Cline and J. D. Hays, Eds., *Geol. Soc. Am. Mem.* **145** (1976).
6. August and February SST data for the modern ocean were digitized on a grid with 2° by 2° spacing by D. Hahn of the Geophysical Fluid Dynamics Program, Princeton University. The data sources are *World Atlas of Sea Surface Temperatures* (Publ. 225, U.S. Navy Hydrographic Office, Washington, D.C., ed. 2, 1944), and *Monthly Charts of Mean, Minimum and Maximum Sea Surface Temperature of the Indian Ocean* (Spec. Publ. 99, U.S. Navy Oceanographic Office, Washington, D.C., 1967).
7. W. L. Prell, W. H. Hutson, D. F. Williams, A. W. H. Bé, in preparation. Sea-surface temperature estimates for February and August conditions at 18,000 years B.P. are based on planktonic foraminiferal transfer function FI-2, which is discussed in W. H. Hutson and W. L. Prell (*J. Paleontol.*, in press).
8. J. D. Hays, personal communication.
9. K. Wyrtki, in *Ecological Studies, Analysis and Synthesis*, B. Zeitzschel, Ed. (Springer-Verlag, New York, 1973), vol. 3; *U.S. Navy Marine Climatic Atlas of the World*, vol. 3, *Indian Ocean* (Government Printing Office, Washington, D.C., 1976).
10. W. L. Prell, W. H. Hutson, D. F. Williams, *Mar. Micropaleontol.*, in press.
11. P. J. Webster and N. A. Streten, *Quat. Res. N.Y.* **10**, 279 (1978).
12. W. L. Prell, in *Evolution of Planetary Atmospheres and Climatology of the Earth* (Centre National d'Etudes Spatiales, Nice, France, 1979), p. 149.
13. W. L. Gates, *Science* **191**, 1138 (1976).
14. S. Manabe and D. G. Hahn, *J. Geophys. Res.* **82**, 3889 (1977).
15. We thank J. Imbrie, T. Webb, and A. McIntyre for their comments on the manuscript. Supported by NSF grant OCE77-22888 to W.L.P. and NSF grant OCE77-23162 to W.H.H.

9 May 1979; revised 6 July 1979

BK Virus DNA: Complete Nucleotide Sequence of a Human Tumor Virus

Abstract. *The complete DNA sequence of the human papovavirus BK is presented. From the 4963 base-pair sequence of BK virus (MM strain), the amino acid sequence of at least five proteins can be deduced: a T antigen and a t antigen, which share amino terminal peptides; proteins VP2 and VP3, which share 232 amino acids; and protein VP1, whose coding sequence overlaps those for VP2 and VP3 by 113 nucleotides but is read in a different frame. The gene loci and the arrangement of genes are strikingly similar in BK virus and simian virus 40 (SV40). The sequence of the deduced proteins in BK virus shares 73 percent amino acid homology with those in SV40, whereas the DNA sequence of the two viruses shares 70 percent homology, suggesting close evolutionary relationship. However, the repeated DNA sequences in the noncoding regions of these viruses are different.*

BK virus (BKV) is a virus of human origin discovered by Gardner *et al.* (*1*). A variant of BKV, termed the MM strain, was later isolated (*2*) from the brain tumor and the urine of a patient with Wiskott-Aldrich syndrome, a genetic disorder characterized by defects of the immune system. This disease has been associated with a high incidence of malignancies of the reticuloendothelial system (*3*). The evidence for the human origin of BKV and BKV(MM) includes their isolation from humans, the preferential growth of the virus in human cells (*4, 5*), and the presence of BKV-specific antibodies in 70 percent of the adult population (*6-8*). The genome of BKV is a closed circular duplex DNA molecule of 3.45×10^6 daltons, whereas that of BKV(MM) is 3.26×10^6 daltons (*9*). Howley *et al.* showed, by hybridization analysis and physical mapping (*9*), that BKV (prototype or wild type) and BKV(MM) are essentially identical. We have constructed more detailed physical maps of the genomes of wild-type BKV(WT) and BKV(MM) and have found differences only between map positions 0.52 and 0.71 (*10*).

Both BKV and SV40 are primate papovaviruses. Each genome consists of only 5200 base pairs. The simplicity of the viral genome and the limited coding capacity require that they depend on host enzymes for replication, transcription, and translation. Because of the close relation with their host cells, these viruses are useful models for understanding gene action and the regulation of transcription and translation in more complex eukaryotic cells.

In human fetal cells BKV reproduces lytically. It can also transform normal hamster cells in vitro as well as produce tumors in vivo when injected into hamsters (*7, 11, 12*). One consequence of productive infection of human cells by BKV is the induction of nuclear tumor antigen (T antigen) that reacts with serum from animals bearing BKV-induced tumors (*7*). The T antigen has been implicated as an important factor in the initiation of viral DNA synthesis and in the induction and maintenance of transformation (*13, 14*). Tumor antigens induced in virus-infected cells or transformed cells by BKV or SV40 are similar, since each reacts strongly with the

0036-8075/79/1026-0456$00.50/0